Charm and beauty structure of the proton

Contribution to the proceedings of HQL06, Munich, October 16th-20th 2006

Riccardo Brugnera[1]
Dipartimento di Fisica dell'Universitá di Padova and
INFN Sezione di Padova
E-mail:riccardo.brugnera@pd.infn.it

1   Introduction

Heavy quarks production is an important testing ground for quantum chromodynamics (QCD), because QCD calculations are expected to be reliable if a hard scale is present in the process. In heavy quarks production a hard scale is provided by the quark mass. Moreover heavy quarks production can give direct access to the gluon density in the proton due to the fact that it proceeds, in QCD, almost exclusively via photon-gluon fusion, where a photon from the incoming electron interacts with a gluon in the proton giving an heavy quark-anti-quark pair. Results will be shown both for deep-inelastic scattering (DIS), where the virtuality of the exchanged boson Q^2 is large, and photo-production, where the Q^2 is equal to zero. Various experimental techniques are used in order to select charm and beauty events, ranging from the measurement of D^* cross section to impact parameter analyses. The results are found to be compatible with the predictions of perturbative QCD (pQCD).

This paper is organized as follows. The relevant features of the HERA collider and of the H1 and ZEUS detectors are described in section 2. In section 3, an introduction to the physics of heavy quarks production in ep collisions is given. The sections 4 and 5 illustrate the tagging methods and the experimental results for the charm quark, while 6 and 7 do the same for the beauty quark. The charm and beauty structure functions are presented in section 8. The results obtained for the gluon polarization by the COMPASS Collaboration are described in section 9. Finally the conclusions are drawn in section 10.

---

[1]On behalf of the H1 and ZEUS Collaborations.

1

2 The HERA collider and its two multipurpose experiments: H1 and ZEUS

HERA is the first *ep* collider and consists of two separate rings of circumference 6.3 km, one a warm magnet electron (or positron) ring with maximum energy 30 GeV and the other a superconducting magnet proton ring of maximum energy 920 GeV. The rings are brought together at four intersection regions, two of them are occupied by the experiments H1 and ZEUS. The HERA life can be divided in two parts: HERA-I from 1992 to 2000 and HERA-II from 2003 to the middle of 2007. During the first period, HERA worked with $e^{\pm}$ beam of 27.5 GeV while the energy of the proton beam was raised from 820 GeV to 920 GeV. The beam spot had the dimension of 150×30 μm^2 and the integrated luminosity collected by each experiments was about 130 pb^{-1}. At the end of 2000 there was a long shutdown, in which both HERA and the two experiments made important upgrades. In 2003 HERA started its functioning and it is to foreseen to work up to the middle of 2007. During the HERA-II period the energies of the lepton and proton beams remained unchanged: 27.5 GeV and 920 GeV respectively. A reduced beam spot (80×20 μm^2) and more reliable beams operation have enhanced a lot the delivered luminosity to the experiments ($\sim$ 180 pb^{-1} per experiment from 2003 to 2005). In Fig. 1 the integrated luminosities per period are shown as function of the day of the run.
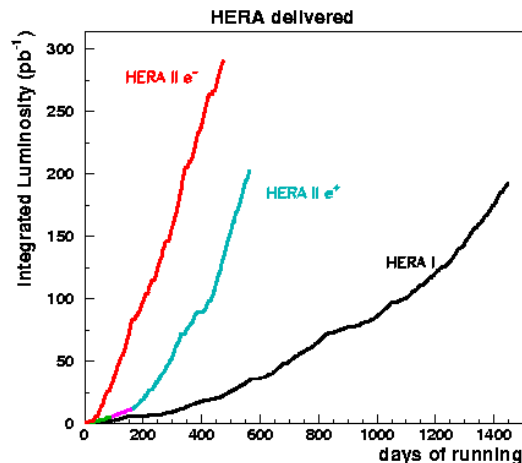

Figure 1: The integrated luminosity delivered by HERA, subdivided into HERA-I period and HERA-II, versus the days of running. The HERA-II period is furthermore divided in HERA-II with electrons (HERA-II e^-) and HERA-II with positrons (HERA-II e^+).

The H1 [1] and ZEUS [2] detectors are general purpose detectors with nearly her-

metic calorimetric coverage. They are designed in order to investigate all aspects of high energy ep collisions. In particular both the scattered electron and the hadronic system in a hard ep interaction are measured. They are differentiated principally by the choices made for the calorimetry. The H1 collaboration has stressed electron identification and energy resolution, while the ZEUS Collaboration has put its emphasis on optimizing calorimetry for the hadronic measurements. The detector designs reflect these different emphases. The H1 detector has a large diameter magnet encompassing the main liquid argon calorimeter, while the ZEUS detector has chosen a uranium-scintillator sampling calorimeter with equal response to electrons and hadrons. Cross sectional view of the H1 and ZEUS detectors are presented in Fig. 2 and 3 respectively.
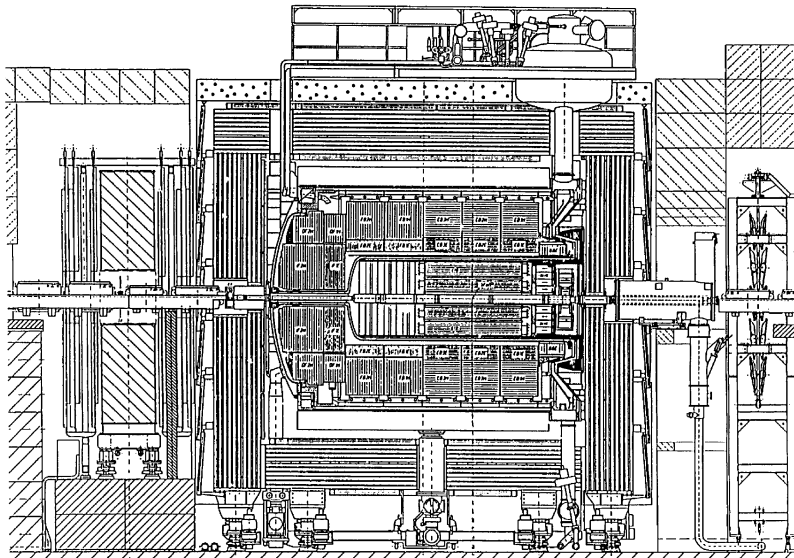

Figure 2: Cross sectional view of the H1 detector.

3 Production of Heavy Quarks in ep collisions

In pQCD, at leading order (LO), two distinct classes of processes contribute to the production of heavy quarks (charm and beauty) in ep collisions at HERA. In direct-photon processes (Fig. 4a), the photon emitted from the electron enters the hard process $\gamma g \to Q\overline{Q}$ directly. In resolved-photon processes (Fig. 4b to 4d), the photon fluctuates into a hadronic state before the hard interaction and acts as a source of partons, one of which takes part in the hard interaction. Resolved photon processes
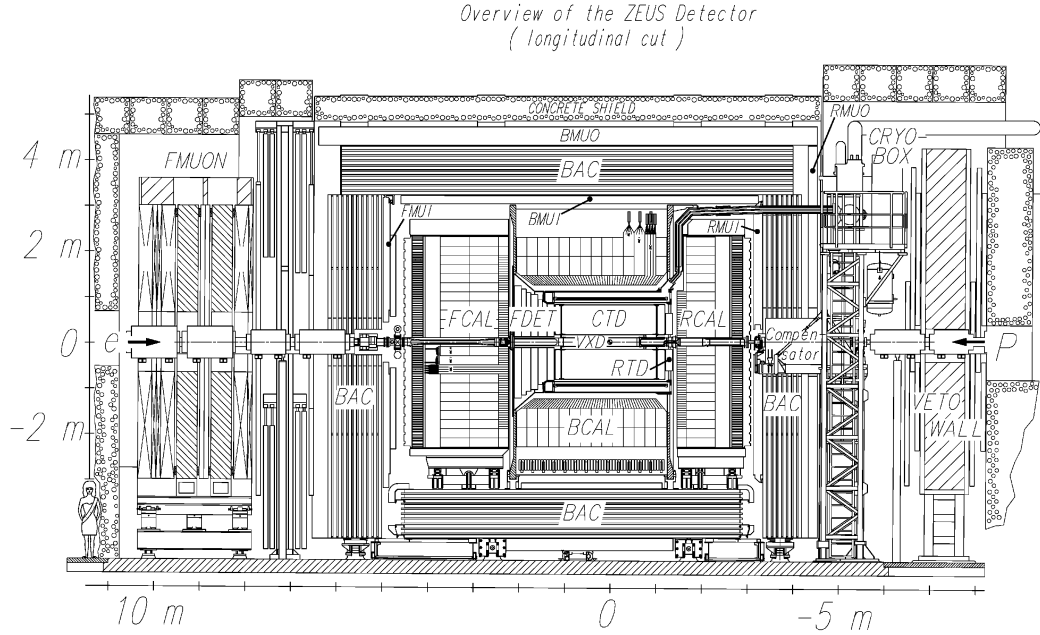
Figure 3: Cross sectional view of the ZEUS detector.

are expected to contribute significantly in the photo-production regime, in which the photon is quasi-real, and to be suppressed towards higher Q^2.

Next-to-leading order (NLO) calculations in several schemes are available [3, 4]. In DIS regime, all approaches assume that Q^2 and heavy quark mass m_Q provide a hard enough scale to allow the applicability of pQCD and to garantee the validity of the factorization theorem. In photo-production regime the hard scale is given by the transverse momentum of the heavy quark $p_{t,Q}$ and m_Q. In the fixed-order, or "massive", scheme [2], u, d, s are the only active flavours in the structure functions of the proton and photon. The heavy quarks are assumed to be produced only at perturbative level via photon-gluon fusion. This scheme is expected to work well in regions where $p_{t,Q}^2 \sim m_Q^2$ (if in photo-production regime) or where $Q^2 \sim m_Q^2$ (if in DIS regime). At higher transverse momenta or Q^2, calculations based on this scheme can break down due to large logarithms $\sim ln(p_{t,Q}^2/m_Q^2)$ ($\sim ln(Q^2/m_Q^2)$). In this case the resummed, or "massless", scheme [3] [5] should be applicable. In this scheme, charm and beauty are regarded as active flavours (massless partons) in the structure functions of the proton and photon and are fragmented from massless partons into massive hadrons after the hard process. There are also calculations[4] which tempt to

---

[2]The scheme is often referred to as fixed flavour number scheme (FFNS).

[3]The scheme is often referred as the zero mass variable flavour number scheme (ZMVFNS).

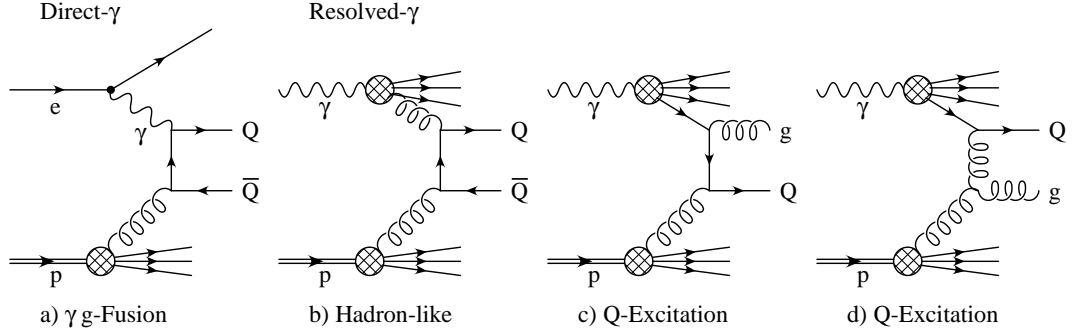[4]The scheme is commonly referred to as variable flavour number scheme (VFNS).

4

Figure 4: Heavy Quarks production processes in leading order pQCD.

treat the heavy quarks correctly for all Q^2. Therefore, at low Q^2, an heavy quark is produced dynamically through the boson-gluon fusion process, whereas, at high Q^2, heavy quark parton densities are introduced. The transition between the two extremes is treated in different way by different authors [6].

4 Charm production: tagging methods

The main method used for charm tagging is the identification of the D^* mesons using the decay channel $D^{*+} \rightarrow D^0 \pi_s^+$ with the subsequent decay $D^0 \rightarrow K^- \pi^+$, where π_s refers to the low momentum π in the decay. The decay particles of the D^* meson are reconstructed in the central detector, usually without particle identification. In Fig. 5 it is shown a distribution of the mass difference $\Delta M = M(K\pi\pi_s) - M(K\pi)$ from the ZEUS Collaboration. A clear signal is seen around the nominal value $M(D^*) - M(D^0)$. In order to mantain under control the combinatorial background, various cuts are made on the p_t of the tracks and on the energy of the event. Of course also other charmed hadrons were identified and analyzed, such as D^+, D_s, Λ_c, but with less statistics. Finally, the sistematic use of the vertex detectors, first implemented in H1 and now also in ZEUS, is changing dramatically the perspective of the physical analysis in the charm sector as it already happened in the beauty one (see section 6 and 7).
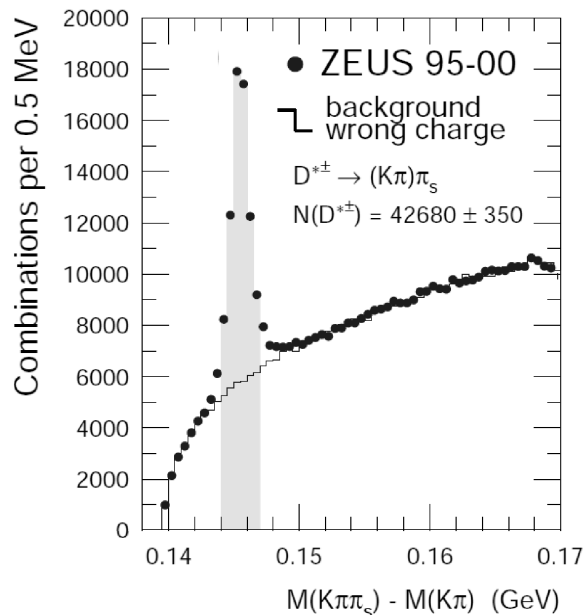
Figure 5: The distribution of the mass difference, $\Delta M = M(K\pi\pi_s) - M(K\pi)$, for D^* candidates. The $D^{*\pm}$ candidates (dots) are shown compared to the wrong charge combinations (histogram). The shaded region shows the signal region. The number of D^* mesons is determined by subtracting the wrong charge background.

5 Charm production: experimental results

The status of the charm analysis can be summarized by the two plots of Fig. 6, where the differential D^* cross section as a function of the pseudo-rapidity[5] of the D^* mesons, $\eta(D^*)$ on the left, and the differential D^* cross sections as a function of Q^2 on the right are shown [7].

The plot on the left of Fig. 6 shows the good agreement between the ZEUS and H1 data. The bands in both plots represent the NLO predictions using the HVQDIS program [8], the widths of the bands correspond to the uncertainties in the mass of the charm, in the renormalization and factorization scales, in the proton parton density functions and in the fragmentation. Rather remarkable is the fact that the $d\sigma/dQ^2$ data are well described by NLO calculations over five orders of magnitude. Some discrepancies between data and theory are seen in photoproduction: D^* photoproduction cross sections [9] as function of the transverse momentum, $p_T(D^*)$, and $\eta(D^*)$ show that the predictions from NLO QCD are too low for $p_T(D^*) > 3$ GeV and $\eta(D^*) > 0$. Part of this deficit may be due to hadronisation effects. The predictions

---

[5]The pseudo-rapidity η corresponding to a polar angle θ (measured respect to the positive z-axis, corresponding to the the incoming proton beam direction) is given by $\eta = $ -ln $\tan(\theta/2)$.
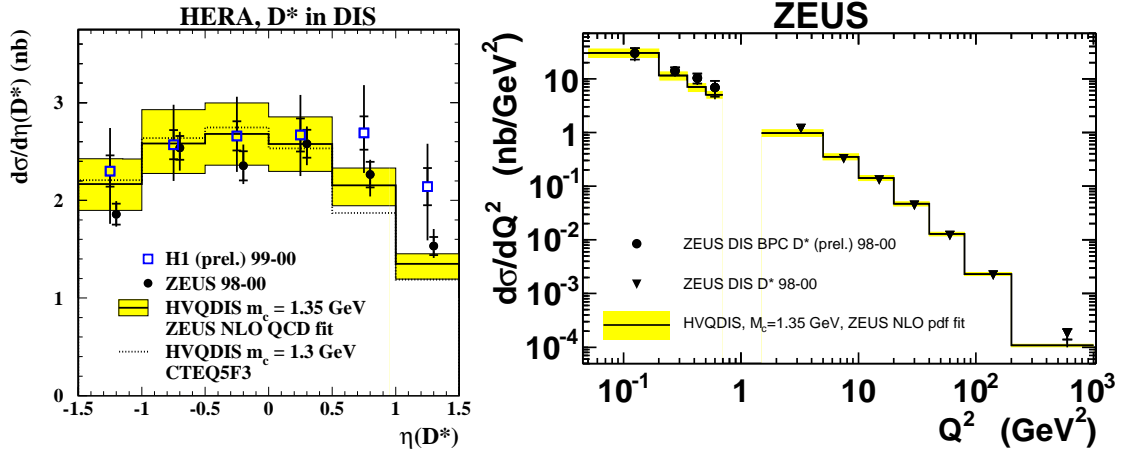
Figure 6: On the left, differential D^* cross sections as a function of $\eta(D^*)$, filled points from the ZEUS experiment and empty squares from the H1 experiment. The bands are the NLO predictions of HVQDIS. On the right, differential D^* cross sections as a function of Q^2 for low Q^2 (dots) and from results on D^* production in DIS (triangle) compared to the NLO predictions from HVQDIS. The data come from the ZEUS Collaboration.

for single jet and dijet production accompanied by a D^* meson should have smaller uncertainties from these effects. For that aim the following correlations were studied: the difference in the azimuthal angle, $\Delta\phi(D^*,\text{jet})$, between the D^* and a jet not containing the D^* meson and those between the two jets of highest transverse energy, $\Delta\phi^{jj}$, and the squared transverse momentum of the dijet system, $(p_T^{jj})^2$. For the LO $2 \to 2$ process, the two jets, or the D^* and a jet not containing the D^* meson, are produced back-to-back with $\Delta\phi = \pi$ and very low p_T. Large deviations from these values may come from higher-order QCD effects. In Fig. 7 the differential cross section as function of the $\Delta\phi(D^*,\text{jet})$ is shown, a large fraction of the produced D^*+jet combinations deviates from back-to-back configuration indicating the importance of higher order contributions. The available NLO calculations (massive FMNR [4] and ZMVFNS [10]) underestimate significantly the observed cross sections in the region $\Delta\phi(D^*,\text{jet})< 120^o$. The cross section $d\sigma/d\Delta\phi^{jj}$, see Fig. 8, is reasonable reproduced by the NLO predictions in the direct-enriched region, that is $x_\gamma^{obs} > 0.75^6$, although the data exhibit a somewhat harder distribution. In the resolved-enriched region, $x_\gamma^{obs} < 0.75$, the data exhibit a harder spectrum than for $x_\gamma^{obs} > 0.75$. The NLO prediction of the cross section for $x_\gamma^{obs} < 0.75$ has a significantly softer distribution compared to the data. The low- x_γ^{obs} region is more sensitive to higher-order topologies not present in the massive NLO prediction. The predictions from PYTHIA MC

---

[6]x_γ^{obs} represents the fraction of the photon momentum partecipating to the hard scattering.

[11] reproduce neither the shape nor the normalisation of the data for low and high x_γ^{obs}. However, the predictions from the HERWIG MC [12] give an excellent description of the shapes of all distributions, although the normalisation is underestimated by a factor of 2.5. The fact that a MC programme incorporating parton showers can successfully describe the data whereas the NLO QCD prediction cannot indicates that the QCD calculation requires higher orders. Matching of parton showers with NLO calculations such as in the MC@NLO programme [13], which is not currently available for the processes studied here, should improve the description of the data.
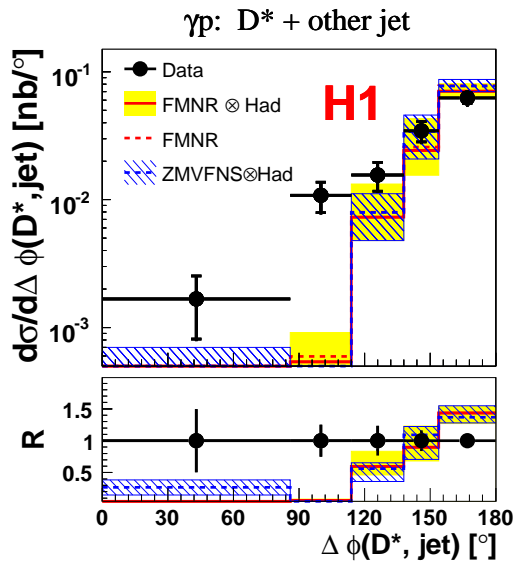

Figure 7: D^*+jet cross sections as function of $\Delta\phi(D^*,\text{jet})$ compared with the predictions of the NLO calculations FMNR and ZMVFNS.

6 Beauty production: tagging methods

The H1 and ZEUS Collaborations have presented measurements in which the events containing beauty are identified in the following manners: using high p_T leptons (mainly muons) from semileptonic b-decays, or using the impact parameters of all tracks coming from secondary decay vertices (inclusive lifetime tag analysis), or finally using double tagged events ($D^* + \mu$, $\mu\mu$).

In the first method, the transverse momentum p_T^{rel} of the muon with respect to the axis of the associated jets exhibits a much harder spectrum for muons from b-decays than for the other sources. Sometime, in order to enhance the signal to noise ratio also the signed impact parameter δ of the muon track with respect to the primary
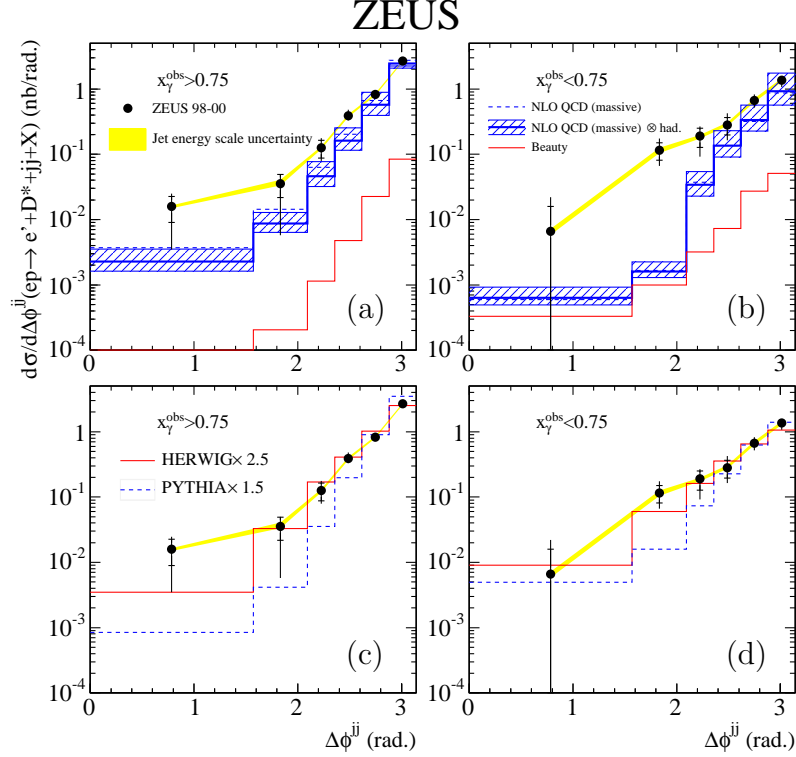
8

Figure 8: Cross section for the process $ep \rightarrow e + D^* + jj + X$ separated into (a,c) direct enriched ($x_\gamma^{obs} > 0.75$) and (b,d) resolved enriched ($x_\gamma^{obs} < 0.75$). The data (solide dots) are compared (a,b) to the massive QCD prediction with (solid line) and without (dotted line) hadronisation corrections applied. The theoretical uncertainties (hatched band) come from the change in scales simultaneously with the change in charm mass. The beauty component is also shown (lower histogram). The data are also compared (c,d) with HERWIG (solid line) and PYTHIA (dashed line) MC predictions multiplied by the indicated factors. The data come from the ZEUS Collaboration.

event vertex is used, this quantity reflects the lifetime of the particle from which the muon decays. The relative contributions from b, c and light quarks are determined by a fit to the p_T^{rel} distribution or to a combined fit to the p_T^{rel} and δ distributions using the shapes of Monte Carlo b, c and light quarks distributions as templates.

In the second method, the track selection requires full silicon vertex detector information. From the measured impact parameter δ a lifetime significance $S = \delta/\sigma_\delta$ is calculated. Two independent distributions are constructed. S_1 is the significance distribution of tracks in events with exactly one selected tracks. S_2 contains the significances of the tracks with the second highest significance for events with two or

more selected tracks. Events in which the tracks with the first and second highest absolute significance have different signs are removed from the S_2 distribution. The subtracted significance distributions are obtained by bin-wise subtraction of the numbers of entries on the negative side from those on the positive side. The subtraction method substantially reduces the systematic uncertainties due to track and vertex resolutions. The relative contributions from b, c and light quarks are determined from a fit to the subtracted S_1 and S_2 distributions and the total number of events, using the shapes of Monte Carlo b, c and light quarks distributions as templates.

In the third method, doubled tagged events, events are selected containing at least one reconstructed D^* and at least one muon, $D^* + \mu$, or two muons in the final state ($\mu\mu$). In order to suppress the various types of backgrounds the charge and angle correlations of the D^* with respect to the muon and of the two muons are exploited. These double tagged measurements extend to significantly lower centre-of mass energies of the $b\bar{b}$ system than measurements based on leptons and/or jets with high transverse momentum. Furthermore, these double tagged events permit to test higher order QCD effects. For instance, in the photon-gluon rest frame the angle between the heavy quarks is 180° at leading order, but at NLO it can differ significantly from this value due to hard gluon radiation.

7 Beauty production: experimental results

Differential measurements from H1 and ZEUS are available for beauty production in photoproduction and DIS [14], [15] using the lepton+jet(s) tag method. Figure 9 shows the differential photoproduction cross sections as a function of the muon transverse momentum (on the left) and of the pseudo-rapidity for the process $ep \rightarrow eb\bar{b}X \rightarrow ejj\mu$. The H1 and ZEUS data, which are in reasonable agreement when they are compared in the same phase space region (see the $d\sigma/d\eta^\mu$ plot on the right side), are compared to a NLO calculation in the massive scheme [4]. The NLO calculations describe the ZEUS data well. Comparing with the H1 data, the NLO calculations predict a less steep behaviour for the $d\sigma/dp_t^\mu$ and is lower than the H1 data in the lower momentum bin by roughly a factor of 2.5; at higher transverse momenta better agreement is observed. In DIS (data not shown), the total cross section measurements made by the H1 and ZEUS Collaborations are somewhat higher than the predictions. The observed excess is pronounced at large muon pseudo-rapidities, low values of Q^2 and muon transverse momentum.

As said in section 6, using double tagged events [16, 17] it is possible to measure the b production up to very low p_t values. In Fig. 10 the differential cross sections as a function of the muon transverse momentum p_T^μ (plot on the left) and the muon pseudo-rapidity η^μ (plot on the right), for muons from b decays in dimuon events and restricted to the phase space $p_t^\mu > 1.5$ GeV and $-2.2 < \eta^\mu < 2.5$ for both
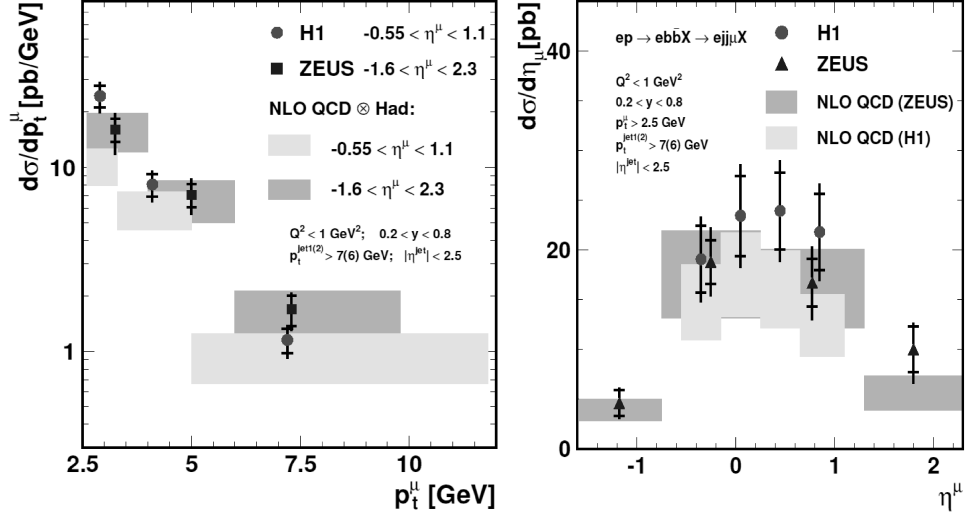
Figure 9: Differential cross sections as a function of the muon transverse momentum p_T^μ (on the left) and the muon pseudo-rapidity η^μ (on the right), for muons coming from b decays in dijet events. The two sets of data coming from the H1 and ZEUS experiments were measured in different phase space regions. The full error bars are the quadratic sum of the statistical (inner part) and systematic uncertainties. The bands represent the NLO predictions convoluted with their uncertaintites obtained by varying the b-quark mass and the renormalization and factorization scales.

muons are shown. Very good agreement is observed with the PYTHIA+RAPGAP [18] predictions scaled by a factor 1.95 (histogram). Apart from the normalization, the leading parton shower approach yields a good description of the corresponding physics processes within the entire accessible phase space. The data are also compared to the absolute NLO prediction in the massive scheme convoluted with the hadronization from PYTHIA MC (shaded band). Again, good agreement in shape is observed, with a tendency to underestimate the data normalisation. A potential trend for increasing data/theory deviations towards low p_t and/or high η, suggested by other measurements as said before, is not supported.

Exploiting the experimental possibilities offered by its microvertex detector, H1 has measured charm and beauty photoproduction using events with two or more jets at high transverse momentum [19]. In this analysis events containing heavy quarks are distinguished from light quark events by the long lifetime of c and b flavoured hadrons, which lead to the displacements of tracks from the primary vertex (see section 6). This analysis provides the first simultaneous measurement of charm and beauty in photoproduction, extending to larger values of transverse jet momentum than previous measurements. In Fig. 11 the measured differential cross sections for
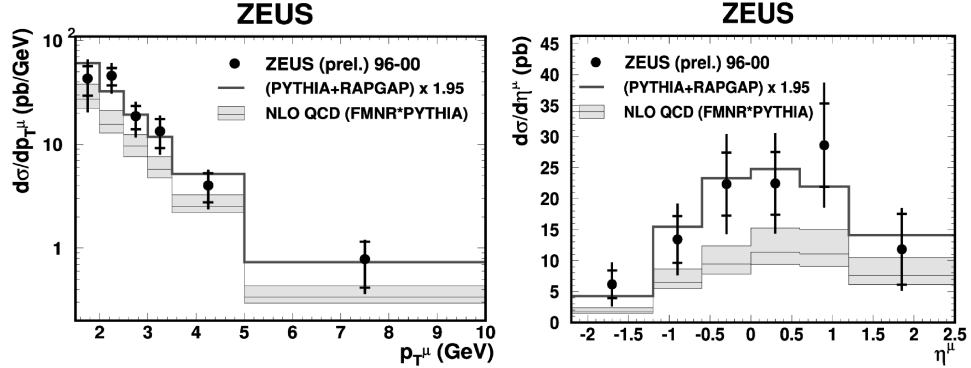
11

Figure 10: Differential cross sections as a function of the muon transverse momentum p_T^μ (on the left) and the muon pseudo-rapidity η^μ (on the right), for muons from b decays in dimuon events. Data come from the ZEUS experiment. The full error bars are the quadratic sum of the statistical (inner part) and systematic uncertainties. The data are compared to the NLO QCD predictions (shaded band) and to the MC predictions (histogram).

charm (plot on the left) and beauty (plot on the right) as functions of the transverse momentum of the leading jet $p_t^{jet_1}$ are shown. Both charm and beauty data are reasonbly well described in shape both by the Monte Carlo simulations (PYTHIA and CASCADE[7] [20]) and the NLO QCD (FMNR) calculations. For charm, the NLO QCD calculation is somewhat lower than the measurement but still in reasonable agreement within the theoretical errors, for beauty the disagreement is slightly higher. The MC's predict a normalisation which is similar to that of FMNR. The bulk of the disagreement between data and NLO calculation, especially for the beauty, is observed in the region of small values of x_γ^{obs} where the prediction lies below the data. Restricting the data to $x_\gamma^{obs} > 0.85$, a significant improvement can be obtained: the charm cross sections are in good agreement with the NLO QCD calculation both in normalisation and shape, the beauty cross sections are also reasonably well described.

The major part of the results shown in this section were obtained in the photoproduction regime ($Q^2 < 1$ GeV^2), and they differ greatly due to different experimental cuts, different tagging-methods. It is difficult to compare each other and also to extract a general message from the comparison between data and NLO QCD calculations. In order to overcome these difficulties the various measured cross sections were

---

[7]The CASCADE program implements the k_t-factorisation approach instead of the usual collinear factorisation approach. In the $\gamma g^* \to Q\overline{Q}$ matrix element, which takes the heavy quark mass into account, the incoming gluon is treated off mass-shell and can have a finite transverse momentum. The calculations are performed at LO, higher order QCD corrections are simulated with initial state parton showers.
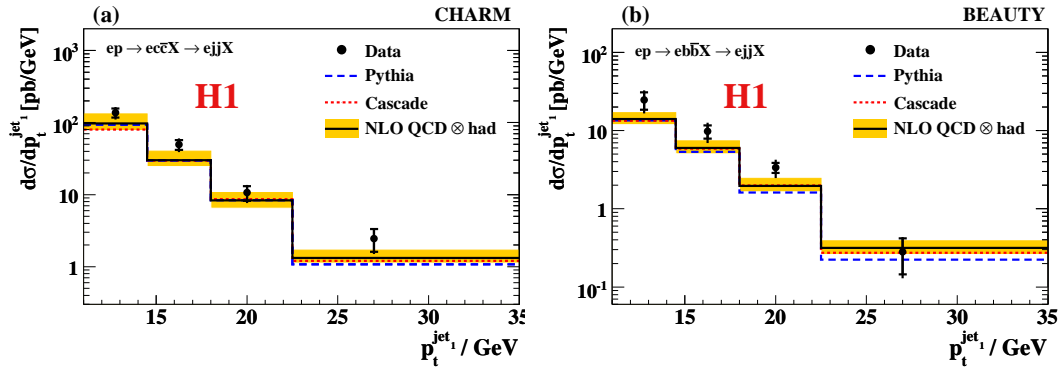
Figure 11: Differential charm (on the left) and beauty (on the right) photoproduction cross sections $d\sigma/dp_t^{jet_1}$ for the process $ep \to e(c\bar{c} \text{ or } b\bar{b})X \to ejjX$. The full error bars are the quadratic sum of the statistical (inner part) and systematic uncertainties. The solid lines indicate the prediction from a NLO QCD calculation, corrected for hadronisation effects, and the shaded band shows the estimated uncertainty. The absolute predictions from PYTHIA (dashed lines) and CASCADE (dotted lines) are also shown.

translated to b-quark differential cross sections as a function of the quark transverse momentum, $d\sigma(ep \to bX)/dp_T^b$, in the pseudo-rapidity range $|\eta^b| < 2$. In Fig. 12 the so extrapolated differential cross sections are shown and compared with the NLO QCD (FMNR) calculations (shaded band). The data are in reasonable agreement between them, they tend to be somewhat higher than the predictions, the disagreement is concentrated at low and medium values of p_T^b, at high values there is a nice agreement.

8 The charm and beauty structure functions

The structure functions more frequently studied (F_2 and xF_3) are inclusive objects and thus contain contributions from both valence and sea quarks. The H1 and ZEUS detectors have the ability to provide identification of a particular quark flavour opening so the possibility of studying the contribution of that flavour to F_2. This is particularly important in the case of heavy flavours, as they are likely produced in the hard scattering and not in the subsequent hadronisation of the struck parton. In other words very precise theoretical predictions can be done as explained in the section 3. Due to the fact that at order α_s heavy quark production in DIS occurs through boson-gluon fusion process (see Fig. 4), this process involves the gluon density xg directly so it gives an experimental handle on this quantity.

$F_2^{c\bar{c}}$ is calculated from the measured charm cross sections as follows:
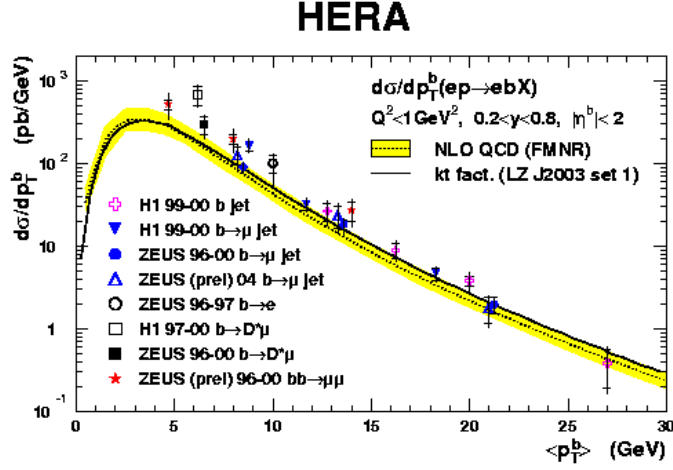
HERA

Figure 12: Differential cross section for b-quark production as a function of the b-quark transverse momentum p_T^b for b-quark pseudo-rapidity $|\eta^b| < 2$ and for $Q^2 < 1$ GeV^2, $0.2 < y < 0.8$. The various points show results from the H1 and ZEUS Collaborations using different b-tag methods. The full error bars are the quadratic sum of the statistical (inner part) and systematic uncertainties. The dashed line shows the NLO QCD prediction with the theoretical uncertainty shown as the shaded band. The continuous line shows the k_t factorization predictions from CASCADE MC.

- The cross section for $c\bar{c}$ is calculated from the D^* cross section [21] (extrapolated to the full phase space) using:

$$\sigma(ep \rightarrow ec\bar{c}X) = \frac{1}{2}\frac{\sigma(ep \rightarrow eD^*X)}{P(c \rightarrow D^*)} \tag{1}$$

where $P(c \rightarrow D^*)$ is the probability that a charm quark will produce a D^* meson (about 25%). As said in the sections 4 and 6, the advent of the micro-vertex detectors has permitted to distinguish events containing heavy quarks from light quark events by the long lifetimes of c and b flavoured hadrons, which lead to displacements of tracks from the primary vertex. Furthermore the results can be obtained in kinematic regions where there is little extrapolation needed to the full phase space and so the model dependent uncertainty due to the extrapolation is small. These measurements were done by the H1 Collaboration [22].

- Finally $F_2^{c\bar{c}}$ is related to $ep \rightarrow ec\bar{c}X$ cross-section by:

$$\frac{d^2\sigma(c\bar{c})}{dxdQ^2} = \frac{2\pi\alpha^2}{Q^4 x}((1 + (1-y)^2)F_2^{c\bar{c}} - y^2 F_L^{c\bar{c}}), \tag{2}$$

14

where the small contribution from $F_L^{c\bar{c}}$ is calculated from QCD, while xF_3 is neglected due to the fact that the measurements are made at small Q^2.

In Fig. 13 (plot on the left) all the data about $F_2^{c\bar{c}}$ are shown as function of x at Q^2 values between 2 and 500 GeV^2. The various data sets, obtained with different techniques, are in good agreement between them. The structure function $F_2^{c\bar{c}}$ shows a rise with decreasing x at constant values of Q^2. The rise becomes steeper at higher Q^2. The data are compared to calculations using the recent ZEUS NLO fit [23], in which the parton densities in the proton are parameterized by performing fits to inclusive DIS measurements from ZEUS and fixed-target experiments. The prediction describes the data well for all Q^2 and x except for the lowest Q^2, where some difference is observed. In Fig. 13 (plot on the right) the ratio $F_2^{c\bar{c}}/F_2$ is shown as function of x at fixed values of Q^2. The charm contribution to F_2 rises from 10% to 30% as Q^2 increases and x decreases. The strong rise of $F_2^{c\bar{c}}$ at low values of x is similar to that of the gluon density and thus supports the hypothesis that charm production is dominated by the boson-gluon fusion mechanism.

Using the help of the micro-vertex detector it was possible to measure the structure function $F_2^{b\bar{b}}$ [22] in a similar manner to those depicted for the $F_2^{c\bar{c}}$. The measurement of the b cross section (and so of $F_2^{b\bar{b}}$) is particularly challenging since b events comprise only a small fraction (typically $< 5\%$) of the total cross section. In Fig. 14 the measured $F_2^{b\bar{b}}$ (by the H1 Collaboration) is shown as function of Q^2. The measurement shows positive scaling violations which increase with decreasing of x. The data are compared with the variable flavour number scheme QCD predictions from MRST [24] and CTEQ [25] at NLO and a recent calculation at NNLO [26]. The predictions are found to describe the data reasonably well. The beauty contribution to F_2, in the present kinematic range, increases rapidly with Q^2 from 0.4% at $Q^2 = 12$ GeV^2 to 1.5% at $Q^2 = 60$ GeV^2.

9   Polarized gluon distribution

In this section, results obtained by the COMPASS Collaboration [27] on the determination of the polarized gluon distribution Δg using the open charm processes in polarized deep inelastic scattering are presented. Formally, one may write for the spin of the proton:

$$\frac{1}{2} = \frac{1}{2}\Delta\Sigma + \Delta g + <L_z>, \tag{3}$$

where $\Delta\Sigma$ is the contribution from the quarks and antiquarks, Δg from the gluons and the last term the mean contribution of any orbital angular momentum of the constituents. While for $\Delta\Sigma$ the situation starts to be solid, the challenge remains to measure Δg and $<L_z>$. The COMPASS experiment at CERN is a facility for spectroscopy and spin physics using hadron and muon beams from the SpS with a
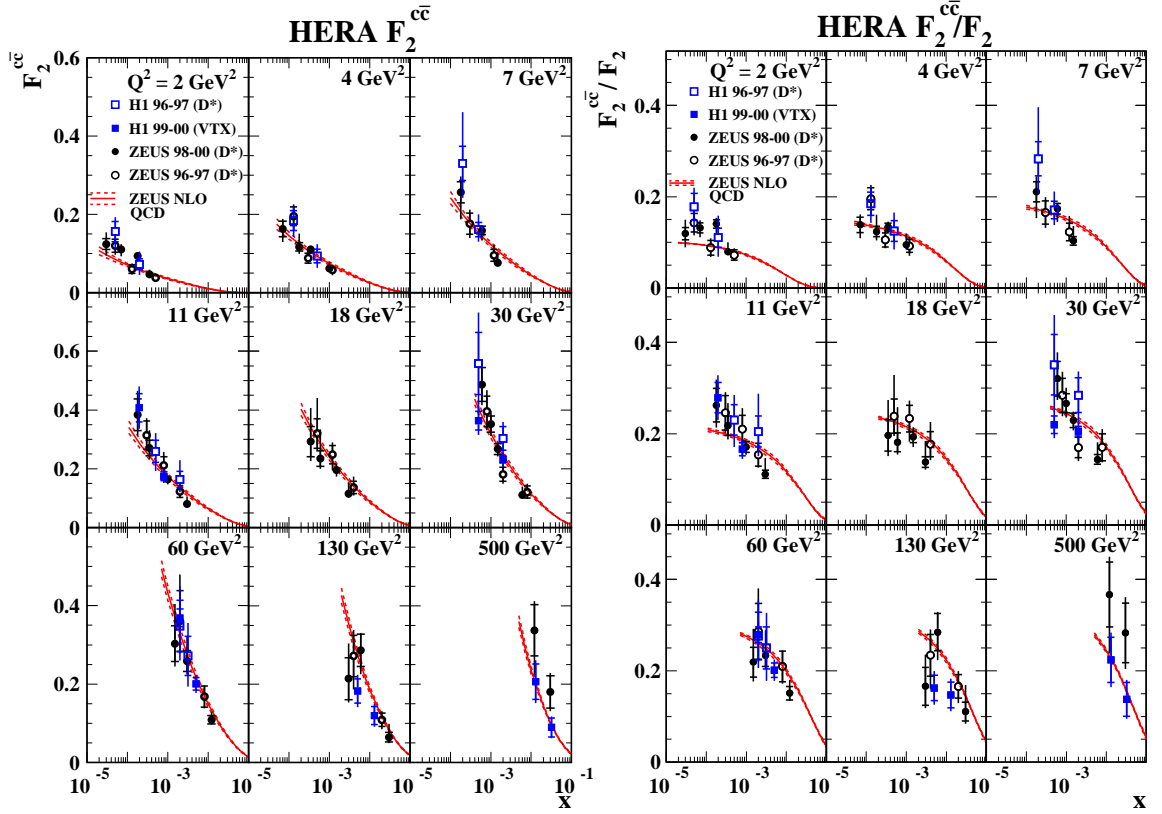
Figure 13: On the left plot, the measured $F_2^{c\bar{c}}$ at Q^2 values between 2 and 500 GeV^2 as a function of x is shown while on the right plot the measured ratio $F_2^{c\bar{c}}/F_2$. Data from the H1 and ZEUS experiments using different charm tagging are shown. The data are shown with statistical uncertainties (inner bars) and statistical and systematic uncertainties added in quadrature (outer bars). The curves represent the ZEUS NLO fit.

variety of targets and a range of sophisticated detectors for analyzing the final state. With a wide range of particle identification devices, the measurement of Δg through the boson-gluon fusion production of $c\bar{c}$ pairs is a primary aim. This first measurement was performed by scattering a positive muon polarized beam at 160 GeV on a solid polarized target. COMPASS has searched for D^o mesons in the decay $D^o \to K^- \pi^+$. To reduce background the neutral D's was also tagged by requiring them to come from the decay $D^{*+} \to D^o \pi^+$. In the measurement there is no reconstruction of the D^o vertex, all the reconstruction is based on the determination of the invariant mass and in the identification of the kaon through the RICH detector. The result is $\Delta g/g = -0.57 \pm 0.41$(stat) at a x value of the gluon equal to 0.15 and at a $Q^2 = 13$ GeV^2; the systematic error is smaller than the statistical one. In Fig. 15 the gluon
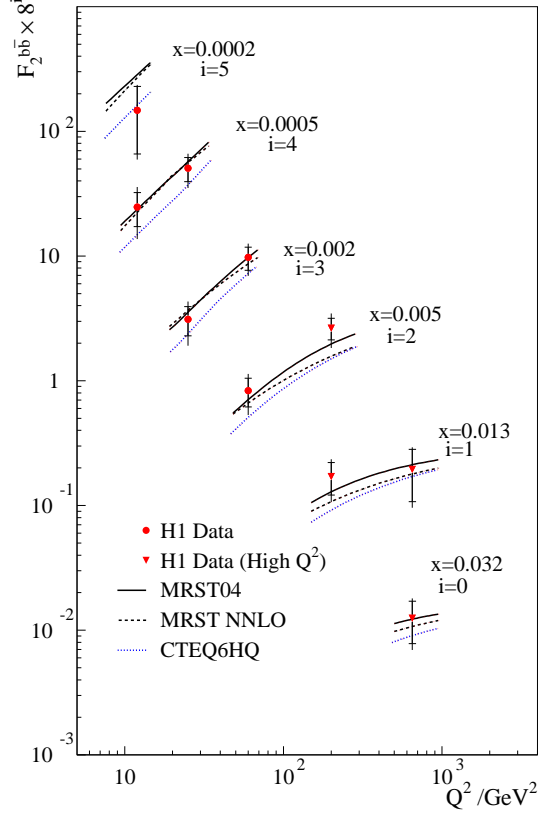
Figure 14: The measured $F_2^{b\bar{b}}$ shown as function of Q^2 for various x values. The inner error bars show the statistical errors, the outer error bars represent the statistical and systematic errors added in quadrature. The prediction of QCD are also shown.

polarization $\Delta g/g$ as a function of x at fixed Q^2 is shown. The points represent the present LO analyses of hadron helicity asymmetries (mainly from high p_T hadrons). The result from open charm obtained by COMPASS is also shown (star symbol). It is smaller than - but still compatible with - zero. COMPASS performed a NLO fits to the spin-dependent structure function $g_1(x, Q^2)$ world data. Two about equally good solutions for $\Delta g(x, Q^2)$ were found, one with a positive and one with a negative first moment ΔG.

10   Conclusions

In the previous pages, part of the results obtained by the H1 and ZEUS Collaborations in the field of heavy flavours has been summarized. We have seen that their charm
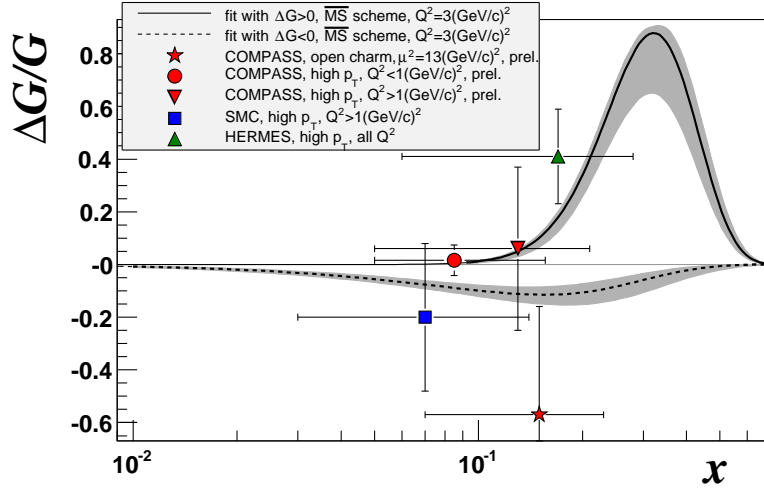
Figure 15: Gluon polarization $\Delta g/g$ as a function of x at $Q^2 = Q_0^2$ obtained by NLO QCD fits (bands) and from LO analyses of hadron helicity asymmetries (symbols).

and beauty data are in satisfactory agreement. In photo-production regime, beauty and charm data are in general agreement with the NLO predictions, even if beauty data are partially slightly higher. Charm production gives a large contribution to the inclusive DIS cross section: it was measured with good precision in a large part of phase space, NLO QCD calculations describe the data within accuracy. The first $F_2^{b\bar{b}}$ measurement was also shown. All the presented results come from the HERA-I period, much more will come using all the statistics from HERA-II period. In the polarized DIS field the new preliminary result on $\Delta g/g$ from the COMPASS Collaboration using open charm was shown. The measurement, considered the most model-independent tool to study gluon-polarisation, still suffers from big statistical uncertainties, they will be highly reduced using the large amount of data that COMPASS will collect in the near future.

References

[1] H1 Collab., I. Abt et al., Nucl. Instrum. Meth. A **386**, 310 (1997).

[2] ZEUS Collab., U. Holm (ed.), *The ZEUS Detector*. Status Report (unpublished), DESY (1993), available on http://www-zeus.desy.de/bluebook/bluebook.html.

[3] E. Laenen et al., Phys. Lett. B **291**, 325 (1992);
E. Laenen et al., Nucl. Phys. B **392**, 162 (1993);

E. Laenen et al., Nucl. Phys. B **392**, 229 (1993);
S. Riemersma, J. Smith and W.L. van Neerven, Phys. Lett. B **347**, 143 (1995);
B.W. Harris and J. Smith, Nucl. Phys. B **452**, 109 (1995);
B.W. Harris and J. Smith, Phys. Lett. B **353**, 535 (1995) [Erratum-ibid B **359**, 423 (1995)];
M.A. Aivazis et al., Phys. Rev. D **50**, 3102 (1994);
J.C. Collins, Phys. Rev. D **58**, 094002 (1998).

[4] S. Frixione et al., Phys. Lett. B **348**, 633 (1995);
S. Frixione et al., Nucl. Phys. B **454**, 3 (1995).

[5] J. Binnewies, B.A. Kniehl and G. Kramer, Z. Phys. C **76**, 677 (1997);
B.A. Kniehl, G. Kramer and M. Spira, Z. Phys. C **76**, 689 (1997);
J. Binnewies, B.A. Kniehl and G. Kramer, Phys. Rev. D **58**, 014014 (1998).

[6] H. L. Lai and W. K. Tung, Z. Phys. C **74**, 463 (1997);
R. S. Thorne, J. Phys. G **25**, 1307 (1999);
A. Chuvakin et al., Eur. Phys. J. C **18**, 547 (2001);
R. S. Thorne and R. G. Roberts, Eur. Phys. J. C **19**, 339 (2001).

[7] ZEUS Collab., S. Chekanov et al., Phys. Rev. D **69**, 0120004 (2004);
ZEUS Collab., *Measurement of D^* meson production in deep inelastic ep scattering at low Q^**, abstract:265, submitted to the XII International Symposium on Lepton-Photon Interactions at High Energy, 30 June - 5 July 2005, Uppsala, Sweden;
H1 Collab., *Inclusive $D^{*\pm}$ meson and associated dijet production in deep-inelastic scattering*, abstract: 5-0163, submitted to the 32nd International Conference on High Energy Physics, ICHEP04, 16 August - 22 August 2004, Beijing, China.

[8] B.W. Harris and J. Smith, Phys. Rev. D **57**, 2806 (1998).

[9] ZEUS Collab., J. Breitweg et al., Eur. Phys. C **6**, 67 (1999);
ZEUS Collab., S. Chekanov et al., Nucl. Phys. B **729**, 492 (2005);
H1 Collab., A. Aktas et al., DESY-06-110, submitted to Eur. Phys. J. C.

[10] B. A. Kniehl, *Hadron Production in Hadron Hadron and Lepton Hadron Collisions*, in *14th Topical Conference on Hadron Collider Physics*, eds. M. Erdmann and T. Mueller, pp. 161-170. Springer, Heidelberg, 2003;
G. Heinrich and B.A. Kniehl, Phys. Rev. D **70**, 094035 (2004).

[11] T. Sjostrand et al., Comp. Phys. Comm. **135**, 238 (2001).

[12] G. Marchesini et al., Preprint Cavendish-HEP-99/17 (1999).

[13] S. Frixione and B.R. Webber, JHEP **0206**, 029 (2002);
S. Frixione, P. Nason and B.R. Webber, JHEP **0308**, 007 (2003).

[14] H1 Collab., C. Adloff et al., Phys. Lett. B **467**, 156 (1999);
H1 Collab., A. Aktas et al., Eur. Phys. J. C **41**, 453 (2005).

[15] ZEUS Collab., S. Chekanov et al., Phys. Rev. D **70**, 012008 (2004);
ZEUS Collab., S. Chekanov et al., Phys. Lett. B **599**, 173 (2004).

[16] H1 Collab., A. Aktas et al., Phys. Lett. B **621**, 56 (2005);
ZEUS Collab., S. Chekanov et al., DESY-06-166, submitted to Eur. Phys. J. C.

[17] ZEUS Collab., S. Chekanov et al., *Measurement of beauty production from dimuon events at HERA*, abstract:269, submitted to the XII International Symposium on Lepton-Photon Interactions at High Energy, 30 June - 5 July 2005, Uppsala, Sweden.

[18] H. Jung, Comp. Phys. Comm. **86**, 147 (1995).

[19] H1 Collab., A. Aktas et al., DESY-06-039, accepted by Eur. Phys. J. C.

[20] H. Jung and G.P. Salam, Eur. Phys. J. C **19**, 351 (2001);
H. Jung, Comp. Phys. Comm. **143**, 100 (2002).

[21] H1 Collab., C. Adloff et al., Z. Phys. C **72**, 593 (1996);
ZEUS Collab., J. Breitweg et al., Phys. Lett. B **407**, 402 (1997);
H1 Collab., C. Adloff et al., Nucl. Phys. B **545**, 21 (1999);
ZEUS Collab., J. Breitweg et al., Eur. Phys. J. C **12**, 35 (2000);
H1 Collab., C. Adloff et al., Phys. Lett. B **528**, 199 (2002);
ZEUS Collab., S. Chekanov et al., Phys. Rev. D **59**, 012004 (2004).

[22] H1 Collab., A. Aktas et al., Eur. Phys. J. C **40**, 349 (2005);
H1 Collab., A. Aktas et al., Eur. Phys. J. C **45**, 23 (2006).

[23] ZEUS Collab., S. Chekanov et al., Phys. Rev. D **67**, 012007 (2003).

[24] A.D. Martin et al., Eur. Phys. J. C **39**, 155 (2005).

[25] S. Kretzer et al., Phys. Rev. D **69**, 114005 (2004).

[26] R.S. Thorne, Phys. Rev. D **73**, 054019 (2006).

[27] See the web site http://wwwcompass.cern.ch/ for any detail.